Nat Hazards
DOI 10.1007/s11069-012-0522-9

ORIGINAL PAPER

# Spatial pattern of landslides in Swiss Rhone Valley

**Marj Tonini · Andrea Pedrazzini · Ivanna Penna · Michel Jaboyedoff**

Received: 17 August 2012 / Accepted: 10 December 2012


**Abstract** The present study analyses the spatial pattern of quaternary gravitational slope deformations (GSD) and historical/present-day instabilities (HPI) inventoried in the Swiss Rhone Valley. The main objective is to test if these events are clustered (spatial attraction) or randomly distributed (spatial independency). Moreover, analogies with the cluster behaviour of earthquakes inventoried in the same area were examined. The Ripley's K-function was applied to measure and test for randomness. This indicator allows describing the spatial pattern of a point process at increasing distance values. To account for the non-constant intensity of the geological phenomena, a modification of the K-function for inhomogeneous point processes was adopted. The specific goal is to explore the spatial attraction (i.e. cluster behaviour) among landslide events and between gravitational slope deformations and earthquakes. To discover if the two classes of instabilities (GSD and HPI) are spatially independently distributed, the cross K-function was computed. The results show that all the geological events under study are spatially clustered at a well-defined distance range. GSD and HPI show a similar pattern distribution with clusters in the range 0.75–9 km. The cross K-function reveals an attraction between the two classes of instabilities in the range 0–4 km confirming that HPI are more prone to occur within large-scale slope deformations. The K-function computed for GSD and earthquakes indicates that both present a cluster tendency in the range 0–10 km, suggesting that earthquakes could represent a potential predisposing factor which could influence the GSD distribution.

**Keywords** Ripley's K-function · Landslides · Cluster · Spatial pattern · Swiss Alps

## 1 Introduction

Geological events such as landslides or earthquakes are more frequently clustered both in space and time than randomly distributed (Mukhopadhyay et al. 2004; Jarman 2006). The

M. Tonini (✉) · A. Pedrazzini · I. Penna · M. Jaboyedoff
Faculté des Géosciences et de l'Environnement, Centre de Recherche en Environnement Terrestre (CRET), Université de Lausanne, Quartier (UNIL) - Mouline, Batiment Géopolis, 1015 Lausanne, Switzerland
e-mail: marj.tonini@unil.ch

Published online: 05 January 2013

analysis of their spatial distribution is of paramount importance to understand their predisposing factors, and for prevention and forecasting purposes (Carrara et al. 1991; Guzzetti et al. 1999). From an orogenic scale, geological events can be described as point processes: this allows analysing their spatial distribution and discovering their pattern behaviour. Point processes can be defined as mathematical models for irregular or random point pattern (Stoyan 2006), or as defined by Diggle (2003) as "stochastic mechanisms which generate a countable set of events."

Generally speaking, cluster analysis includes algorithms aiming at grouping objects showing similar properties into the respective categories. A spatial cluster includes events whose density is higher than expected in the surrounding area. This assumption can be accepted or rejected based on the result of random simulations. This type of analysis allows to better understand the data structure and to reject the hypothesis of independency among events. Keefer (1984) showed that landslides triggered by earthquakes have a tendency to occur at well-defined location around the epicentre.

Spatial clusters can be identified whenever the observed distance among point locations in space is lower than the expected distance for a random distribution (e.g. Poisson model). For geological events, which intensity is non-constant along the study area, their cluster detection is not evident. A vast literature exists on the spatial analyses of these events, especially for susceptibility map purpose, in particular for landslides (Lee et al. 2007; Conoscenti et al. 2008; Bai et al. 2010; Nandi and Shakoor 2010; Oh and Lee 2011; Erener and Düzgün 2012), and for earthquakes (Fischer and Horálek 2003; Faenza and Pierdominici 2007; Tsai and Shieh 2008; Ansari et al. 2009; Varga et al. 2012).

In this paper, the importance of applying statistical methods to assess whether or not the spatial distribution of geological point processes satisfies a Poisson point process (Zuo et al. 2009) is emphasised. Despite the large interest in spatial distribution and characterisation of geological events, there is a lack in comprehensive studies as concern the use of statistical methods to assess spatial attraction between the events. Here, a global cluster indicator, namely the Ripley's K-function ($K(r)$), was employed to measure and test for randomness (Ripley 1976). As $K(r)$ depends on the distance $r$ between pairs of events, its application allows describing the spatial point process at many distance values and defining a range at which events are randomly distributed (independency), clustered (attraction) or eventually dispersed (repulsion).

In the present study, the spatial pattern of quaternary gravitational slope deformations (GSD, 294 events) and of historical/present-day instabilities (HPI, 400 events) inventoried in the Swiss Rhone Valley is investigated. The main objective is to test if they are clustered or randomly distributed over increasing distance scales, and if exists a spatial attraction between landslides. Our hypothesis is that GSD and HPI are not randomly distributed and that the two classes of landslides display similar pattern behaviour since they share the same geological context. Moreover, it is well known that the slope instabilities are more susceptible to take place where rock mass strength is reduced such as in ancient landslides. The Ripley's K-function estimation was adopted to validate this hypothesis: it represents a powerful statistical summarising method to test for inter-point "attraction" and "clustering." The $K(r)$ was computed to assess the randomness of GSD and HPI distribution, whilst the cross K-function was computed to prove the attraction between events belonging to these two classes of landslides (Lotwick and Silverman 1982). The pairwise comparison between the K-functions evaluated separately for each group of landslides helped to highlight analogies in their individual spatial patterns. In a final step, the spatial cluster behaviour of gravitational slope deformations and earthquakes was compared to explore if the two datasets follow a similar trend, which could attest for an interaction between the

two phenomena. To account for the natural non-homogeneous distribution of geological events, a generalisation of $K(r)$ to non-stationary point processes (i.e. non-constant intensity at each location) was applied (Baddeley et al. 2000). In fact, it is well known that the spatial pattern of landslides and earthquakes is conditioned from environmental factors that affect their random occurrences. Among them, a common predisposing factor is the tectonic history and the related tectonic fractures, as well as their orientation regarding a free face like a valley slope (e.g. Abele 1974; Keefer 1984; Hermanns and Strecker 1999).

## 2 Geologic and geomorphologic setting

The study area is located in south-west of Switzerland, covering the entire upper sector of the Rhone watershed, from the Rhône river delta on the Lake Geneva to the Rhone sources located in central Swiss Alps. Its extension is of about 5000 km$^2$ (Fig. 1).

The north-western sector of the study area is marked by the presence of the Prealps nappes, characterised by sedimentary rocks (Mosar et al. 1996). The northern part is dominated by the Helvetic nappes, mainly consisting of metamorphic and sedimentary rocks. In the north-east side, the Aar massif basement dominates the zone. In the south, the Penninic domain features the landscape; its outcrops belong to highly deformed crystalline, metasedimentary and ophiolitic rocks. Two major tectonic structures are present in the study area: the Rhone-Simplon fault and the Penninic thrust. The first one belongs to a dextral strike slip fault system whose trace controlled the development of the Rhone Valley (Steck 1984). The Rhone Valley represents among the most seismically active area in central Swiss Alps (Maurer et al. 1997). From 1500 year up to nowadays, more than 2000 earthquakes with moment magnitude higher than two and at least six historical events with

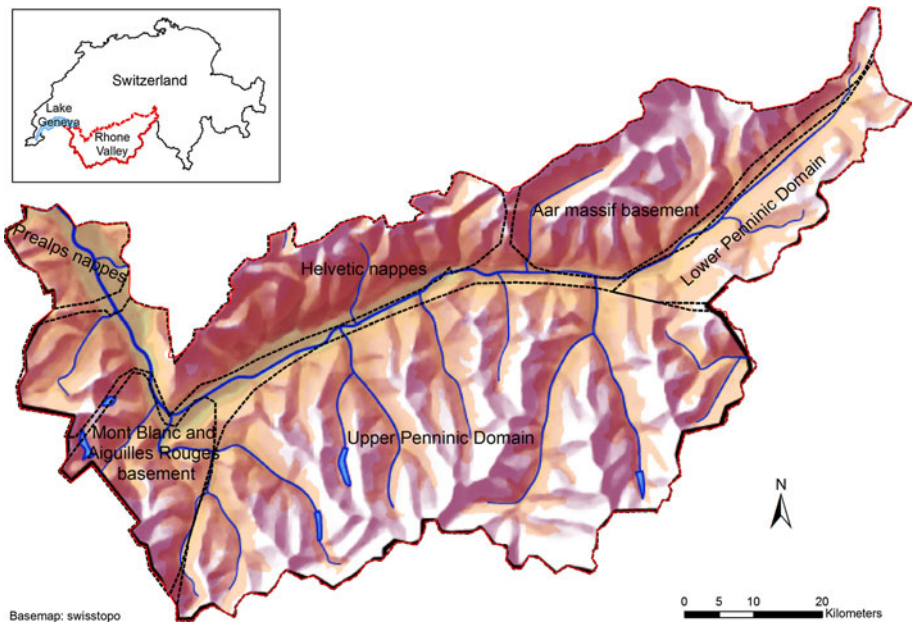


**Fig. 1** The study area: Swiss Rhone Valley and its main tectonic units

an estimated magnitude higher than six were recorded in this area (Faeh et al. 2003). The current landscape's configuration was mainly driven by the alpine glaciation during the last glacial maximum and paraglacial processes that took place after the glacial retreat (Hinderer 2001). Glacial erosion generated an important overdeepening of the Rhone Valley, following the weakness zone of the Simplon fault (Preusser et al. 2010).

## 3 Methods

### 3.1 Data collection

A geodatabase storing information on location and characteristics of gravitational slope deformations (GSD) was implemented at the University of Lausanne, Switzerland (Pedrazzini 2012). Data have been extracted from four different sources:

- Review of scientific and technical studies as well as analysing and digitising features described in the published 1:25000 geological maps (Swisstopo).
- Aerial photographs (1:20000 and 1:30000) and orthophotos (15 and 25 cm pixel size).
- Digital elevation model (Swisstopo) at 2 m/25 m cell size for areas below/above 2000 m asl.
- Google Earth images (© Google 2010).
- Local field mapping.

A lower size limit of 0.05 $km^2$ was retained to provide an inventory as complete as possible and to avoid scale discrepancy between GSD detected from remote sensing data and those extracted from 1:25000 geological maps. A similar size limit was also chosen by Korup (2005); he also proposed to map GSD according to their typology. It is often difficult to assign specific GSD within complicated classical classifications such as Hutchinson (1988) or Cruden and Varnes (1996). Complex sites that can fit several categories are common; hence, Jarman (2006) identified just five broad categories for the Scottish Highlands. Here, landslides have been classified by a three-way simplification of Hutchinson (1988):

1. Deep-seated creep/sagging (DSCS, 142 events) characterised by pronounced scarps and counterscarps and by the presence of different minor landslides inside the deformed mass.
2. Rockslide and rock avalanches (RRA, 91 events) characterised by monolithic masses of rock with a failure surface marked by pre-existing discontinuity sets.
3. Large roto-translation landslides (LRT, 61 events) characterised by distinct headscarps, pronounced toe bulges and debris lobes.

For the scope of the analysis, the centroid of the area covered by each landslide event was considered (Figs. 2, 3).

Historical/present-day instabilities (HPI) consisting in more than 400 events identified during the last century and stored as points in two coordinates. Most of the information derived from the catalogue of the main rock-falls in Switzerland elaborated by the Research Centre on the Alpine Environment (CREALP) (Fig. 3).

Seismic data come from the Earthquake Catalogue of Switzerland 2009 (ECOS-09) elaborated from the Swiss Seismological Service (SED). For the scope of the present analysis, only instrumentally recorded earthquakes with magnitude higher than 3 were considered (Fig. 3). According to Keefer (1984), which study is based on an inventory of

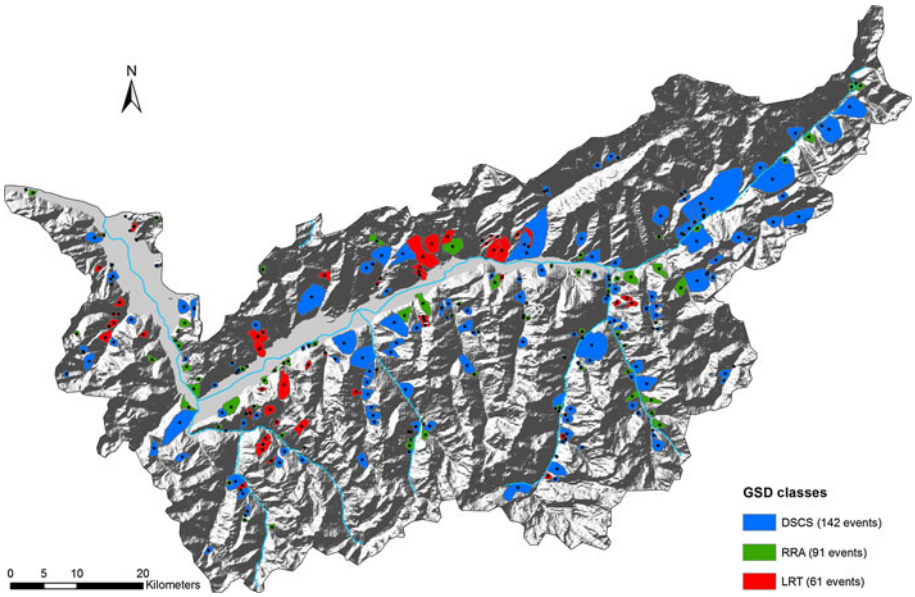


**Fig. 2** Gravitational slope deformations (GSD) inventoried along the Swiss Rhone Valley. The tree main classes are represented: deep-seated creep/sagging (DSCS, in *blue*); large roto-translation landslides (LRT, in *red*); and rockslide and rock avalanches (RRA, in *green*)

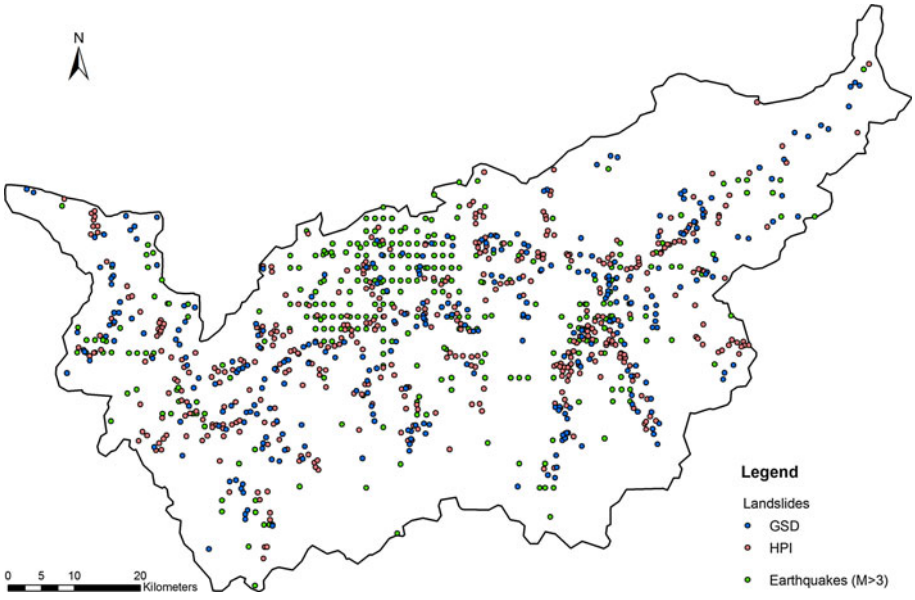


**Fig. 3** Geological events. *Blue dots* represent the centroids of gravitational slope deformations (GSD); *red dots* represent the historical/present-day instabilities (HPI); *green dots* represent instrumentally recorded earthquakes with magnitude higher than 3

historical events, this magnitude represents the lower limit for landslides triggered by earthquakes.

### 3.2 Ripley's K-function

A diagnostic of independence among geological events was performed by means of the Ripley's K-function (Ripley 1976). This statistic exploratory method allows detecting if a point process (e.g. *X*,*Y* location of events) belonging to a given phenomenon is random distributed or if, on the contrary, it exists an attraction (clustering) or a repulsion (dispersion) among data (Dixon 2002).

Analytically, the K-function $K(r)$ equals the expected number of additional points $n$ within a distance $r$ from a randomly distributed event u divided by the intensity $\lambda$:

$$K(r) = \frac{1}{\lambda} E[n(X \cap b(u,r) \backslash \{u\} \mid u \in X)]$$

where the intensity $\lambda$ of the point process $X$ is defined as the average number of points per unit area and $b(u,r)$ is a circle of radius $r$ centred over a point $u$ of $X$ (Fig. 4a).

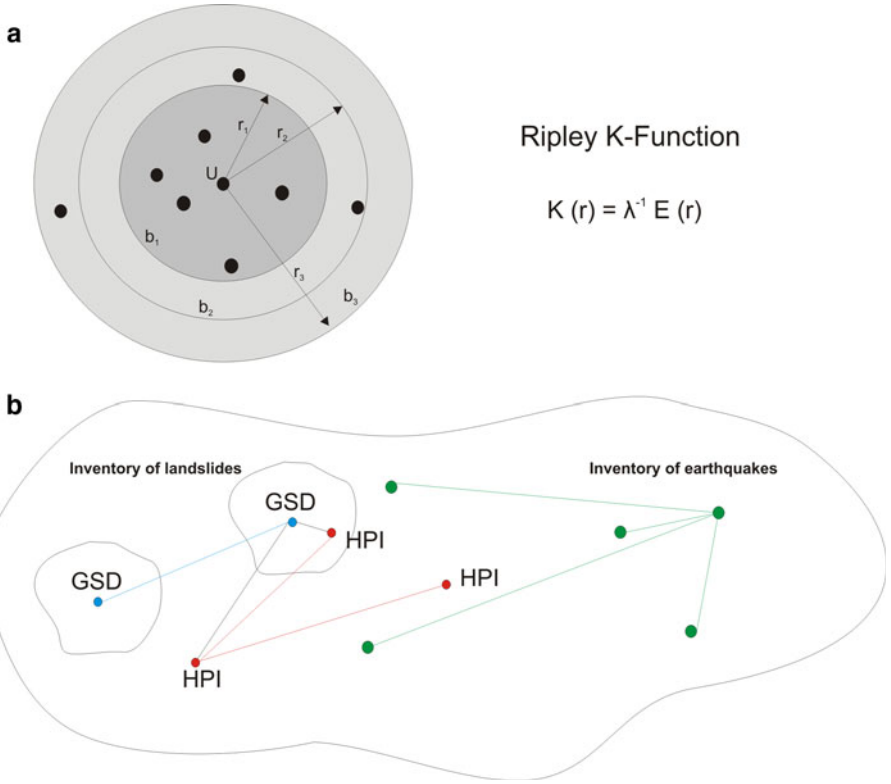


**Fig. 4** The Ripley's K-function analyses point patterns at increasing distance values, as represented by the circles in **a** (see on the text for symbol explanation). The interaction between the different geological events is represented in **b**: gravitational slope deformations (GSD); historical/present-day instabilities (HPI); and earthquakes

Under complete spatial randomness (CSR), which assumes independency among events and a uniform Poisson distribution of events inside any specific sub-area (also referred to a stationary or homogeneous point process), $K(r)$ is equal to $\pi r^2$.

$K(r)$ can be plotted against the distance $r$, so that it is easy to compare the estimated curve with the theoretical one (for CSR): if the estimated $K(r)$ value for a given distance $r$ is higher than $\pi r^2$, then events are spatially clustered, whilst smaller values indicate repulsion between events. That way allows finding out at which range of distance $r$ data perform a non-random pattern distribution (e.g. cluster or dispersion).

The study area where geological events were observed was modelled as the polygon of irregular shape delimiting the Rhone Valley. Since events falling outside this boundary are not counted to calculate the intensity of the phenomenon, edge correction was applied and introduced in the computation of the K-function. Essentially, if a circle falls only partially inside the study area, only the overlapping surface is counted.

A variety of edge-corrected estimators have been proposed in literature. The most commonly used is due to Ripley (1988). Including it in the computation, the $K(r)$ assumes the following form:

$$K(r) = \frac{1}{\lambda} \sum_{i} \sum_{i \neq j} \frac{1}{w(l_i l_j)} \frac{I(d_{ij} < r)}{N}$$

where the weight function, $w(l_i l_j)$, provides the edge correction and $N$ represents the total number of points. Considering $d_{ij}$ the distance between two points $i$th and $j$th, the indicator function ($I$) assumes the value of 1 when the circle of radius $d_{ij}$ is completely inside the study area. If part of the circle falls outside the study area, then $w(l_i l_j)$ corresponds to the proportion of the circumference included inside.

It is important to notice that the intensity of spatial distributed geological events normally varies along the study area, so that they cannot be considered as stationary point processes. Indeed, landslides' distribution is influenced from different morphological and geological factors such as slope and lithology (Guzzetti et al. 1999; Carrara et al. 1991) whose distribution varies along the space. To take into account the local variability of the intensity characterising the phenomena under study, a modification of the K-function for a non-stationary (also said inhomogeneous) point process was adopted (Baddeley et al. 2000). The inhomogeneous K-function assumes that each point $x_i$ is weighted by its local intensity $\lambda(x_i)$. Independently on the location u and considering the indicator function (I), the inhomogeneous K-function is defined as:

$$K_{inhom}(r) = E\left[\sum_{x_i \in X} \frac{1}{\lambda(x_i)} I\{0 < \| u - x_i \| \leq r\} \mid u \in X\right]$$

As for the stationary case, if events are randomly distributed, then $K_{\text{inhom}}(r)$ is equal to $\pi r^2$. Therefore, the same considerations about the comparison between the theoretical and the estimated values assumed by the function are valid. Light of the inhomogeneous distribution of geological events, the use of the inhomogeneous K-function enables to overcome to a misinterpretation between the natural non-constant intensity and a veritable attraction of events (Hering et al. 2009) which represents a clustering.

The assumption of inhomogeneity in landslides and earthquakes distribution was proved via chi-squared test of CSR, using irregular Voronoi tessellation. The study region was divided into sub-regions, and the number of points observed inside each one was compared with the expected number of events under the assumption of homogeneous intensity. This way allows rejecting the null hypothesis at a pre-fixed confidence level.

Many studies attest of landslides reactivations of ancient deposits (Bertolini et al. 2005) and how deep-seated gravitational slope deformations can evolve into hazardous slope collapses (Bonnard et al. 2004). To verify this assumption for our case study, the cross K-function was applied and the spatial dependency of the first class of events (HPI) from the second one (GSD) was considered. Computationally, the pair $K(r)$-cross function counts the number of events belonging to one process arising at a distance $r$ from an event belonging to a second process. As for the standard $K(r)$ function, if the first process is spatially independent from the second one (i.e. randomly distributed around it), then the $K(r)$-cross assume the value $\pi r^2$, whilst deviations between the estimated and the theoretical curve may suggest a spatial interaction (attraction or repulsion) between the two processes.

Actually in the present study, we computed a transformation of the Ripley's K-function, namely the L-function (Besag 1977) which makes it easier to compare the estimated with the theoretical curves and to evaluate departures from this last one. The L-function is defined as:

$$L(r) = \sqrt{\frac{K(r)}{\pi}}$$

The square root has the effect of stabilising the variance of the estimator. For a completely random point pattern distribution, the theoretical value of the L-function minus $r$ always assumes the value zero.

To test for CSR, 999 Monte Carlo simulations of a realisation of an inhomogeneous random point process were performed, and for each simulation, the $L(r)$ function was computed. This provides a pointwise minimum–maximum Monte Carlo envelopes, allowing to judge about data randomisation (the null hypothesis) for each value of $r$. Events are assumed to be random distributed if, for a fixed value of the distance $r$, the empirical $L(r)$ function is included between the upper and the lower simulated curves (i.e. the maximum–minimum envelope). Moreover, the null hypothesis can be rejected if the estimated curve lies outside the envelope. The significance level of this test at each value of $r$ is equal to $2/(1 + \text{number of simulations})$, that is, 0.2 % in our case.

To resume, the K-function was applied to explore if (a) gravitational slope deformations (GSD), historical/present-day instabilities (HPI) and earthquakes inventoried dataset are spatially clustered or randomly distributed; (b) if GSD and HPI are attracted each other; (c) if GSD and earthquakes show similar cluster tendency (Fig. 4b).

All the computations were carried out using R free software for statistical computing and graphics (R Development Core Team 2012). R is a free software environment integrating facilities for data manipulation, calculation and graphical display. The R base can be extended via packages available through the Comprehensive R Archive Network (CRAN) which covers a very wide range of modern statistics. More specifically, the spatial point pattern analyses of the geological events considered in the present study and their cluster detection were supported by the package spatstat (Baddeley and Turner 2005).

## 4 Results

### 4.1 Inhomogeneous data distribution

Geologic events are not-stationary processes whose probability distribution changes in space and in time. For this reason, the inhomogeneous K-function is more appropriate to give a measure of clustering of geological point processes. First of all, the inhomogeneous distribution of the entire dataset (GSD, HPI and earthquakes) was proved via chi-squared

**Table 1** The chi-squared test ($X^2$) for the considered geological phenomena

| Geological events | $X^2$ | $p$ value |
|---|---|---|
| GSD | 23.7881 | 0.0002384 |
| HPI | 11.3291 | 0.04523 |
| Earthquakes ($M > 3$) | 13.7639 | 0.01718 |

The statistical $p$ value is also reported

dispersion test ($X^2$) for spatial pattern based on quadrat counts. The number of observed events ($N_i$) and of expected events ($\bar{N}$) under the assumption of CSR (that implies homogeneity in the spatial distribution of the phenomenon) was calculated for each tessellation on which the study area was subdivided. Then, the $X^2$ test was calculated as follows:

$$X^2 = \sum_{i=1}^{n} \frac{(N_i - \bar{N})^2}{\bar{N}}$$

The values of $X^2$ were computed and compared with the values stated on $X^2$ table. Considering the irregular shape and the orientation of the study area, Dirichlet/Voronoi tessellation instead of regular quadrats was considered. We established to divide the area in 6 sub-regions, which correspond to five degree of freedom, as a compromise to account for global and regional inhomogeneity. Results are shown on Table 1: the null hypothesis of CSR can be rejected with a confidence level ($p$ value) of at least 0.05 or better. Consequently, the intensity of events is to be considered non-constant along the study area.

### 4.2 Gravitational slope deformations

Gravitational slope deformations (GSD) inventoried over the study area were further classified into three groups as described above. $L(r)$ trend for deep-seated creep/sagging (DSCS, 142 events), rockslide and rock avalanches (RRA, 91 events) and large roto-translational landslides (LRT, 61 events) shows that each group of landslides is clustered at a distance ranging from 500 m up to about 11 km with a peak at about 1.5 km (Fig. 5). Each class of instabilities can be individually explored to detect its significant attraction among events over 999 random simulations. The observed $L(r)$ function for each class lies above the upper simulated envelopes in a close range of distance values as follows: 1–1.6 km for LRT, 0.9–2.5 km for the RRA and 1.5–5.5 km for DSCS. The simulation band width is quite high due to the small number of events belonging to each class and the high number of simulations; this is especially evident in the case of LRT. Nevertheless, this analysis assures a significant level of 0.002 at these values of distance.

### 4.3 Gravitational slope deformations and historical/present-day instabilities

The $L(r)$ function computed over the entire dataset representing the gravitational slope deformations (GSD) well describes at which values of distance $r$ events display cluster behaviour. This happens in the range 0.75–9.5 km, whilst events are dispersed above about 18 km and included between the upper and the lower simulated curves in between, meaning a random distribution. Historical/present-day instabilities (HPI) show a similar

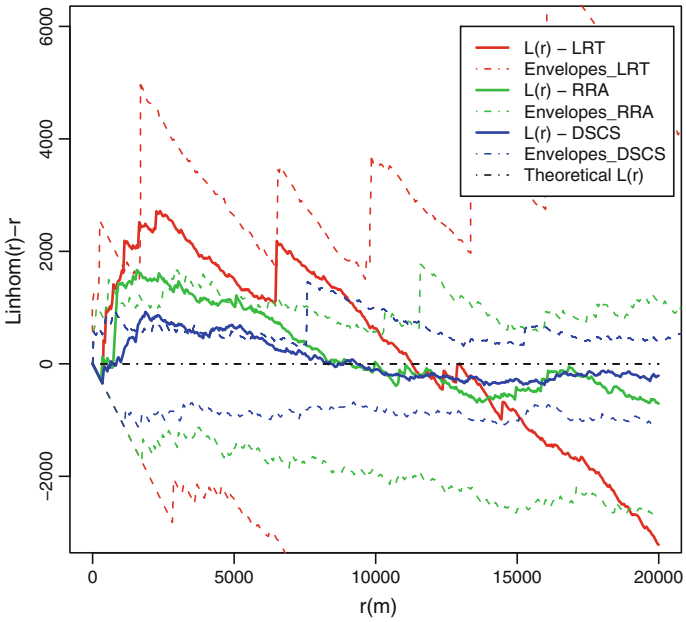


**Fig. 5** The empirical $L(r)$ function computed for large roto-translation landslides (LRT, *red line*), rockslide and rock avalanches (RRA, *green line*), and deep-seated creep/sagging (DSCS, *blue line*). *Dashed lines* represent the minimum–maximum Monte Carlo envelopes computed over 999 simulations. The *black dashed line* represents the theoretical $L(r)$ function

pattern distribution as can be observed by plotting together the $L(r)$ function for the two dataset (Fig. 6): events are clustered from about 0.75 km up to 8.5 km, dispersed above 12.5 km and randomly distributed in between. The comparable trend of the two curves indicates that events belonging to the two types of instabilities could be affected from the same predisposing factors and could be attracted each other and not be independently distributed. Moreover, on our inventoried dataset, 32 % of all HPI follow inside the area covered by GSD.

To test the hypothesis of an attraction between HPI and GSD, the inhomogeneous cross-$L(r)$ function was computed (Fig. 7). The trend of the curve shows a cluster behaviour in the range 0–4 km, proving that at this distance the number of HPI in the neighbourhood of GSD (and vice versa) is higher than expected for an inhomogeneous random distribution of events. From 4 km up to about 7.5 km, the two types of instabilities are independently distributed, whilst above 7.5 km, they are dispersed, meaning repulsion among the different events.

### 4.4 Gravitational slope deformations and earthquakes

The $L(r)$ function was computed to give a measure of clustering of GSDs and earthquakes taking place along a huge time period in the same area, the Rhone Alps Valley. The $L(r)$ trend (Fig. 8) shows that the spatial distribution of landslides and earthquakes is not random and that both geological phenomena are clustered from close to 0 up to about 10 km. This similar trend in the cluster behaviour of the two geological processes can attest an interaction and demonstrate a predisposing factor of earthquakes for GSD.

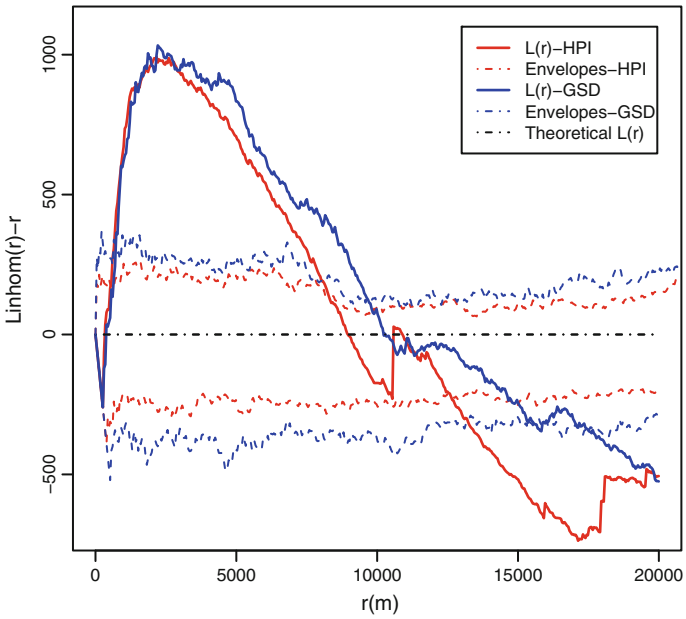


**Fig. 6** The empirical $L(r)$ function computed for historical/present-day instabilities (HPI, *red line*) and gravitational slope deformations (GSD, *blue line*). *Dashed lines* represent the minimum–maximum Monte Carlo envelopes computed over 999 simulations. The *black dashed line* represents the theoretical $L(r)$ function

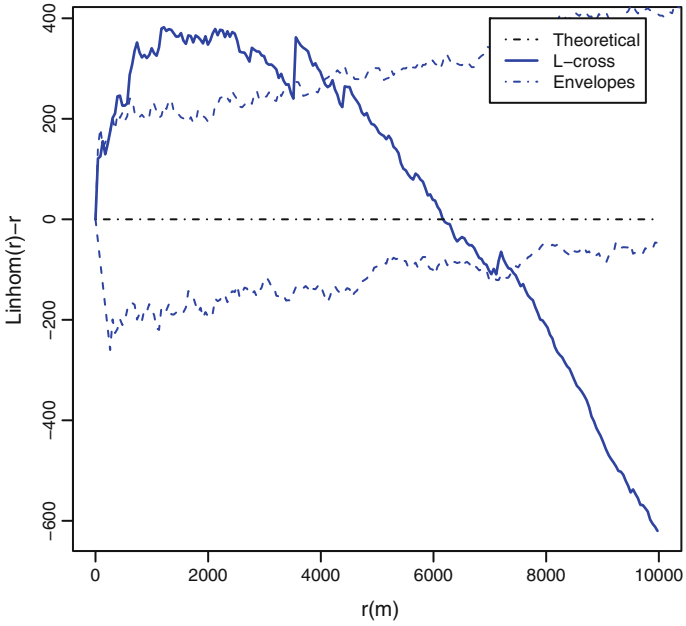


**Fig. 7** The empirical cross-$L(r)$ function computed between gravitational slope deformations and historical/present-day instabilities (*blue line*). *Dashed lines* represent the minimum–maximum Monte Carlo envelopes computed over 999 simulations. The *black dashed line* represents the theoretical $L(r)$ function

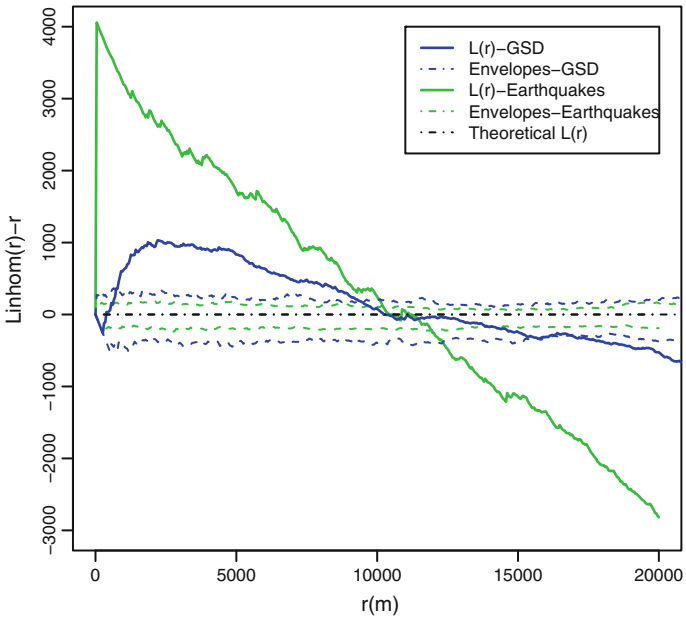


**Fig. 8** The empirical $L(r)$ function computed for gravitational slope deformations (GSD, *blue line*) and earthquakes (*green line*). *Dashed lines* represent the minimum–maximum Monte Carlo envelopes computed over 999 simulations. The *black dashed line* represents the theoretical $L(r)$ function

## 5 Discussion and conclusions

In this paper, we analysed the spatial pattern of landslides and earthquakes recorded in the Swiss Rhone Valley. For the scope of the analyses, geological events were treated as punctual data. Under the assumption of spatial inhomogeneity of the patterns, as naturally is for geological events, the K-function showed evidence of punctual events attraction at well-defined distance values.

The main results coming from the estimated K-function are as follows: (1) gravitational slope deformations, historical/present-day instabilities and earthquakes are spatially clustered over specific ranges of distance; (2) historical/present-day instabilities are spatially attracted from gravitational slope deformations; (3) gravitational slope deformations and earthquakes display a similar pattern behaviour.

The abovementioned results attest for events interaction and lead to interesting interpretations as concern the properties and the genesis of the geological phenomena. The results clearly indicate that landslides are not randomly distributed but spatially attracted in clusters at well-defined distance range and this cluster behaviour is demonstrate over a huge number of simulation envelopes (Monte Carlo test). This analysis represents a global indicator of a cluster spatial distribution; moreover, the detected critical distance values can be retained for future local cluster analyses aiming to locate clusters in space.

The cross K-function trend confirms that the two classes of landslides (gravitational slope deformations and historical/present-day instabilities) are not independently distributed. Indeed, it is well known that modern instabilities are likely to occur within ancient landslides (Bertolini et al. 2005). The revealed spatial relationship between the two classes indicates that the decrease of rock mass strength from quaternary landslide deposits acts as

predisposing factor for new instabilities. This observation of the increase in susceptibility due to the remobilisation of materials in old landslide deposits is relevant for hazard analysis and prevention purposes. In fact, remobilisations represent a well-known threat for infrastructures in Alpine areas, which have produced important economic losses in the past (Bonnard et al. 2004).

Finally, the comparison between the K-functions evaluated separately for gravitational slope deformations and earthquakes reveals a similar cluster behaviour. The comparable spatial pattern of geological phenomena could be indicating that repeated low-magnitude seismic activity acts as a long-term predisposing factor causing a progressive reduction of rock mass strength, in a zone where rocks are also highly fractured due to tectonic efforts along fault zone, and slopes affected by lateral release after the retreat of glaciers. However, the discussion about trigger factors for landslides in the study area is beyond the scope of this study which focuses on their spatial pattern distribution.

**Acknowledgments** This work was partly supported by the SNFS project No. 200021-140658: "Analysis and modelling of space–time patterns in complex regions."

## References

Abele G (1974) Bergstürze in den Alpen: Wissenschaftliche Alpenvereinshefte. Münche Ausschüsse des Deutschen und Österreichischen Alpenvereins 25:231

Ansari A, Noorzad A, Zafarani H (2009) Clustering analysis of the seismic catalog of Iran. Comput Geosci 35(3):475–486

Baddeley A, Turner R (2005) Spatstat: an R package for analyzing spatial point patterns. J Stat Softw 12(6):1–42

Baddeley A, Moller J, Waagepetersen R (2000) Non- and semiparametric estimation of interaction in inhomogeneous point patterns. Stat Neerl 54:329–350

Bai SB, Wang J, Lü G, Zhou P, Hou SS, Xu SN (2010) GIS-based logistic regression for landslide susceptibility mapping of the Zhongxian segment in the three Gorges area, China. Geomorphology 115:23–31

Bertolini G, Guida M, Pizziolo M (2005) Landslides in Emilia-Romagna region (Italy): strategies for hazard assessment and risk management. Landslides 2(4):302–312. doi:10.1007/s10346-005-0020-1

Besag J (1977) Discussion of Dr Ripley's paper. J Roy Stat Soc B 39:193–195

Bonnard C, Forlati F, Scavia C (2004) Identification and mitigation of large landslide risks in Europe: advances in risk assessment. Balkema, Amsterdam, p 317

Carrara A, Cardinali M, Detti R, Guzzetti F, Pasqui V, Reichenbach P (1991) GIS techniques and statistical models in evaluating landslide hazard. Earth Surf Process Landf 16:427–445

Conoscenti C, Di Maggio C, Rotigliano E (2008) GIS analysis to assess landslide susceptibility in a fluvial basin of NW Sicily (Italy). Geomorphology 94(3–4):325–339

Cruden DM, Varnes DJ (1996) Landslide types and processes. In: Turner AK, Shuster RL (eds) Landslides: investigation and mitigation, Transportation Research Board, Special Report 247, pp 36–75

Diggle PJ (2003) Statistical analyses of spatial point patterns, 2nd edn. Arnold, London

Dixon PM (2002) Ripley's K function. In: El-Shaarawi AH, Piergorsch WW (eds) The encyclopedia of environmetrics. Wiley, New York, pp 1796–1803

Erener A, Düzgün HSB (2012) Landslide susceptibility assessment: what are the effects of mapping unit and mapping method? Environmental Earth Sciences 66(3):859–877

Faeh D, Giardini D, Bay F, Bernardi F, Braunmiller J, Deichmann N, Furrer M, Gantner L, Gisler M, Isenegger D, Jimenez MJ, Kästli P, Koglin R, Masciadri V, Rutz M, Scheidegger C, Schibler R, Schorlemmer D, Schwarz-Zanetti G, Steimen S, Sellami S, Wiemer S, Wössner J (2003) Earthquake catalogue of Switzerland (ECOS) and the related macroseismic database. Eclog Geol Helv Swiss J Geosci 96(2):219–236

Faenza L, Pierdominici S (2007) Statistical occurrence analysis and spatio-temporal distribution of earthquakes in the Apennines (Italy). Tectonophysics 439(1–4):13–31

Fischer T, Horálek J (2003) Space-time distribution of earthquake swarms in the principal focal zone of the NW Bohemia/Vogtland seismoactive region: period 1985–2001. J Geodyn 35(1–2):125–144

Guzzetti F, Carrara A, Cardinaly M, Reichenbach P (1999) Landslide hazard evaluation: a review if current techniques and their application in a multi-scale study, Central Italy. Geomorphology 31:181–216
Hering AS, Bell CL, Genton MG (2009) Modeling spatio-temporal wildfire ignition point patterns. Environ ad Ecol Stat 16:225–250
Hermanns RL, Strecker MR (1999) Structural and lithological controls on large Quaternary rock avalanches (sturzstroms) in arid northwestern Argentina. Geol Soc Am Bull 111(6):934–948
Hinderer M (2001) Late quaternary denudation of the Alps, valley and lake fillings and modern river loads. Geodin Acta 14:231–263
Hutchinson JN (1988) General report: morphological and geotechnical parameters of landslides in relation to geology and hydrogeology. In: Bonnard C (ed) Proceedings of the fifth international symposium on landslides. Balkema, Rotterdam, pp 3–35
Jarman D (2006) Large rock slope failures in the Highlands of Scotland: characterisation, causes and spatial distribution. Eng Geol 83:161–182
Keefer DK (1984) Landslides caused by earthquakes. Geol Soc Am Bull 95:406–421
Korup O (2005) Distribution of landslides in southwest New Zealand. Landslides 2(1):43–51
Lee S, Ryu J-H, Kim I-S (2007) Landslide susceptibility analysis and its verification using likelihood ratio, logistic regression, and artificial neural network models: case study of Youngin, Korea. Landslides 4:327–338
Lotwick HW, Silverman BW (1982) Methods for analysing spatial processes of several types of points. J R Statist Soc Ser B 44:406–413
Maurer HR, Burkhard M, Deichmann N, Green AG (1997) Active tectonism in the central Alps: contrasting stress regimes north and south of Rhone Valley. Terra Nova 9:91–94
Mosar J, Stampfli GM, Girod F (1996) Western Prealpes Medianes Romandes; timing and structure; a review. Eclogae Geol Helv 89:389–425
Mukhopadhyay B, Dasgupta S, Dasgupta S (2004) Clustering of earthquake events in the Himalaya—its relevance to regional tectonic set-up. Gondwana Res 7(4):1242–1247
Nandi A, Shakoor AA (2010) GIS-based landslide susceptibility evaluation using bivariate and multivariate statistical analyses. Eng Geol 110:11–20
Oh HJ, Lee S (2011) Landslide susceptibility mapping on Panaon Island, Philippines using a geographic information system. Environ Earth Sci 62:935–951
Pedrazzini A (2012) Characterization of gravitational rock slope deformations at different spatial scales based on field, remote sensing and numerical approaches. PhD Thesis. Institute of Geomatics and Analysis of Risk, University of Lausanne
Preusser F, Reitner J, Schlüchter C (2010) Distribution, geometry, age and origin of overdeepened valleys and basins in the Alps and their foreland. Swiss J Geosci 103:407–427
R Development Core Team (2012) A language and environment for statistical computing. R Foundation for Statistical Computing, Vienna, Austria. URL: http://www.R-project.org/
Ripley BD (1976) The second-order analyses of stationary point processes. J Allied Probab 13:255–266
Ripley BD (1988) Statistical inference for spatial processes. Cambridge University Press, Cambridge, MA
Steck A (1984) Structures de deformations tertiaires dans les Alpes centrales (transversale Aar-Simplon-Ossola). Eclogae Geol Helv 77(1):55–100
Stoyan D (2006) Fundamentals of point process statistics. In: Case studies in spatial point process modeling. Lecture Notes in Statistics 185, Springer, Berlin
Tsai CY, Shieh CF (2008) A study of the time distribution of inter-cluster earthquakes in Taiwan. Phys A 387(22):5561–5566
Varga P, Krumm F, Riguzzi F, Doglioni C, Süle B, Wang K, Panza GF (2012) Global pattern of earthquakes and seismic energy distributions: Insights for the mechanisms of plate tectonics. Tectonophysics 530–531:80–86
Zuo R, Agterberg FP, Cheng Q, Yao L (2009) Fractal characterization of the spatial distribution of geological point processes. Int J Appl Earth Obs Geoinf 1:394–402